Materials Science in Semiconductor Processing 166 (2023) 107729

Contents lists available at ScienceDirect

Materials Science in Semiconductor Processing

journal homepage: www.elsevier.com/locate/mssp

# Impacts of structural downscaling of inorganic molecular crystals - A DFT study of $Sb_2O_3$

Alia Jabeen [a], Abdul Majid [a,*], Mohammad Alkhedher [b], Sajjad Haider [c], Muhammad Saeed Akhtar [d]

[a] Department of Physics, University of Gujrat, Gujrat, 50700, Pakistan
[b] Mechanical and Industrial Engineering Department, Abu Dhabi University, Abu Dhabi, 59911, United Arab Emirates
[c] Chemical Engineering Department, College of Engineering, King Saud University, P.O.Box 800, Riyadh, 11421, Saudi Arabia
[d] School of Chemical Engineering, Yeungnam University, Gyeongsan, 38541, Republic of Korea

ARTICLE INFO

*Keywords:*
Inorganic molecular crystals (IMCs)
$Sb_2O_3$
Density functional theory
Structural properties
Electronic properties
Two dimensional (2D) materials
Downscaling
Inter-cage interactions
Periodic energy decomposition analysis (pEDA)
Electron localization functions (ELF)

ABSTRACT

Inorganic molecular Crystals (IMCs) is an emerging class of two-dimensional (2D) materials having unconnected structural units. In contrast to the conventional 2D materials, $Sb_2O_3$ appears in the form of periodically arranged *van-der-Waals (*vdWs*)* molecular clusters. Besides the specific material's features, IMCs offer unique features due to anisotropy in bonding, packing, electronic and thermal conductivity, and optical characteristics. The work reported herein depicts the modification in structural and electronic properties of $Sb_2O_3$ trimmed from bulk to lower dimensions. The shortening in bond-lengths pointing to variation in inter-cage interactions and decrease in band gap are observed with the structural downscaling. The bulk, slab (111), slab (001) and clusters are semiconductors with the major contribution arising from Sb and O in formation of conduction and valence bands respectively. The electronic properties of the materials pointed to p-p hybridization and hence presence of π-bonding and anti-bonding molecular orbitals within the region present between the molecular cages.

## 1. Introduction

The inorganic molecular crystals (IMCs) has been introduced in 2019 in the form of a new type of 2D vdWs materials comprising of molecular clusters or cages [1,2]. Such type of the vdWs materials are based on spatially isolated inorganic molecules which are connected via vdWs interactions throughout the crystal. This specific crystal configuration has motivated the researchers to develop the strategies in order to synthesize the vdWs films or relevant interfaces and hetero-structures for device applications. However, the synthesis of such crystal structures is challenging task due to several problems particularly when fabrication of large scale and reproducible conventional 2D materials has not yet been established.

Considering to the presence of weak vdWs interaction, the layered materials could be comparable with the IMCs that would aid to study and understand the IMCs. Because of the specific crystal structure of the layered materials with weak vdWs interactions, the layered materials could be synthesized by the mechanical exfoliation [3–6]. This is due to presence of comparatively stronger chemical intralayer bonding but weak interlayer vdWs bonding that helps peeling-off the layers via the exfoliation. In contrast, however, the 2D IMCs could be hardly synthesized via exfoliation of the bulk crystals due to their anisotropic nature [7]. Hence, the IMCs could be obtained in distinct crystallographic planes upon structurally downscaling the bulk. Besides the exfoliation, the commonly employed technique for synthesis of graphene (i.e. layered material) is chemical vapor deposition method which is not equally instrumental to prepare 2D-IMCs [8].

The presence of vdWs interactions in conventional layered materials and 2D IMCs doesn't guarantee the similarity of both the types. The layered materials are different from those of IMCs and these could be distinguished on the basis of anisotropy. In majority cases of IMCs, the cages contain strong covalent bonding with such a configuration that makes them inert i.e. no more atoms can be bonded with the existing structure. This property of the cages which restrict entry of further atoms is not usually available in the conventional layered materials.

The specific molecular configuration bestows the 2D-IMCs to exhibit fascinating characteristics. Considering their diverse structural properties, the improvement in the synthesis strategies as well as the

* Corresponding author.
*E-mail addresses:* Abdulmajid40@yahoo.com, abdulmajid40@uog.edu.pk (A. Majid).

https://doi.org/10.1016/j.mssp.2023.107729
Received 8 March 2023; Received in revised form 4 June 2023; Accepted 8 July 2023
Available online 13 July 2023

exploration of applications based on the IMCs is of prime research interest. Because of insolubility of the inorganic molecules, there are problems to realize the large-size self-assembled 2D IMCs. One of the most famous IMCs is $Sb_2O_3$, which has been successfully synthesized and showed its potential in the several applications such as Li/Na ion batteries and field effect transistors (FETs) [9,10]. Due to the presence of the weak forces, the inorganic molecules could be easily sublime at higher vacuum. During the process of the evaporation, the molecular configuration could also be sustained and in this way the molecules could configure the films that are free from the dangling bonds. The $Sb_2O_3$, because of its wide band gap, is considered to be a high-k-dielectric materials and showed the potential in the vdW dielectric that could assist the integration of the higher yield 2D devices [11].

The properties of the materials are structure dependent and one of the most intriguing aspect of first-principles framework is the access to structure - property relation at atomic/electronic level [12]. In fact, the dawn of the quantum chemistry considers the wave function as well as the intrinsic delocalized picture of the electronic configurations based on the chemical bonding within the solids and molecules. Consequently, the vast variety of the methodologies for the investigations of the electronic configurations has been introduced, which could be vastly categorized in (i) the electronic density in real space, (ii) orbitals based in the Hilbert space, (iii) methodologies to include the modelling of the experimentally observable quantities, (iv) methods based on the energies. These methods have been broadly utilized but often face limitations in the extended systems. One of the most promising technique in this regards is the utilization of the energy decomposition analysis (EDA) [13] on the basis of the effort by Morokuma [14] along with the extension of extended transition state (ETS) presented by the Ziegler and Rauk [15]. Besides this, the extension presented recently introduced the EDA-NOCV (energy decomposition analysis -Natural Orbitals for Chemical Valence) method that provide additional information through the analysis of the energy as well as the charge in combined manner. The other methods includes the crystal orbital overlap populations (COOP) [16], natural bond order (NBO) [17,18], density of states (DOS) and partial density of states (pDOS) etc. The robustness of above mentioned method lies in its capability to evaluate the bonding contributions by the energy terms, out of which the EDA along with NOCV have been utilized for study of the periodic systems.

The nanomaterials exhibited great importance due to their applications in cutting edge technologies and everyday life [19–23]. These materials have quickly gained lime light because of their intriguing properties and novel aspects dependent on their nature, size and morphology. The conventional nanomaterials appear different structures and periodicities, including 3D bulk structures, 2D planar structure like slabs, 1D chains, and 0D clusters or quantum dots. These structures usually appear in form of networks with repetition of unit cell is one, two or three dimensions. However, in contrast to these network structures, the synthesis of inorganic molecular crystals (IMC) based nanomaterials comprising of isolated cages has been reported [2,24]. The molecular units in IMC nanomaterials are not physically bonded but affiliated via van der Waals forces due to which these are expected to offer extra properties in addition to the conventional nanomaterials. In order to realize the IMC nanomaterials, the trimming of their 3D bulks is required. The downscaling of IMC's to lower dimensions to produce slabs, chains and clusters needs to be carried out in order to utilize them for applications. The downscaling of the materials in order to achieve their littler counterparts may lead to novel phenomenon and unknown effects. As the thickness of the films reaches to the nanometer scale, the surface properties, quantum size effects as well as the interfacial phenomenon become prominent [25,26]. The relevant impacts can be understood by investigating the physical properties including structural, mechanical and electronic characters of the materials. One of the motivations to downscale the bulk is to prepare free standing films on suitable substrates with lower interfacial strain, lattice mismatch and other relevant requirements [35].

The process of structural downscaling may lead to large number of novel applications [19]. The materials in lower dimensions are known to exhibit improved performance in microelectronics as the fabrication of transistors appeared to ensure greater density in integrated circuits, economical, lower power consumption and faster response [27]. The inorganic semiconductor nanomaterials are suitable for investigating the nano-scale phenomenon and dimensionality dependent properties. The structural units of the materials formed by the nanoscale inorganic semiconductors with controlled geometries are expected to play an important role in future nano-devices [28]. Furthermore, the IMCs based nanomaterials may offer novel phenomenon in biosensors, drug delivery, bio medicines, fuel cells, sensors, catalysis and hydrogen storage etc. [29].

The downscaling (moving towards lower dimensions) of dimensionality has been done for many materials but the same has not yet been reported for IMCs. Furthermore, owing the specific crystal structure of the IMCs, the downscaling of the bulk of these crystals in lower dimensions may introduce planes of different miller indices. The realization of different surfaces in case of IMCs would have the impact on the orientation of cages and hence offer the structural diversities. Like the conventional crystals, in order to explore the possible applications of the IMCs, their study in different dimensions is essentially required. Considering the ongoing trend in miniaturization of conventional materials, the predictions on trimming of IMCs and its follow-up experimental synthesis is expected to develop technology for future requirements. This work is carried out with motivation to investigate the downscaling of IMCs to attain most stable configuration in the form of slabs, chains and clusters. For this purpose, the bulk $Sb_2O_3$ was trimmed in different orientations to obtain 2D slabs in the form of (i) (111) plane and (001) plane (ii) 1D chains and (iii) 0D clusters. The specific crystal structure of $Sb_2O_3$ motivated the authors to investigate the interactions between the independent molecular units (i.e. cages) by performing the pEDA-NOCV calculations. The structural and electronic properties of the 3D (bulk), 2D slabs in (111) and (001) orientations, 1D chains in (111) and (001) orientations and 0D clusters will be discussed in detail in the coming sections.

## 2. Computational details

The work being reported here describes the structural and electronic properties of $Sb_2O_3$ in bulk, slabs (111), slab (001), chains as well as clusters as derived from slab (111) and slab (001) and hence termed as chains (111), chains (001), clusters (111) and clusters (001) respectively. The unit cell of stable cubic structure of $Sb_2O_3$ was used as an initial structure and completely optimized. The bulk unit-cell contain the 4 formula units with 8 atoms of Sb and 12 atoms of O. The unit-cell for slab (111), chains (111), clusters (111) contains the 40 atoms while the slab (001), chains (001) and clusters (001) contains 80 atoms each. The size of super-cell for the bulk and slab is $2 \times 2 \times 2$ and $2 \times 2$ respectively. The structural and electronic properties of the work was carried out using density functional theory (DFT) based LCAO (Linear combination of atomic orbitals) formulism implemented on ADF-BAND (2022.103) code whereas the dynamical stability of said materials were investigated using Vienna ab-initio simulation package (VASP). The ADF uses Slater type orbitals (STO's) that are well-known for accurate prediction in regions close to nucleus [30]. Triple zeta basis sets were used for the calculations with the confinement radius of 10 Bohr. First of all, the geometry of all the cases were fully relaxed to obtain completely optimized structures. Further, the bulk structure was optimized at three different levels of theory i.e. GGA-PBE, GGA-PBE-D3 and GGA-PBE-D3-BJ. In order to prepare 2D structures, the bulk was sliced in two different ways to produce slabs i.e. along (111) plane and (001) plane. The slabs in the form of unit cells and respective $2 \times 2$ super cells were optimized at all the above described levels of theory. The electronic properties were then computed during single point runs. The

anisotropy is expected for all the cases so the three different level of theories are used and all the calculations are performed using GGA-PBE, GGA-PBE-D3, GGA-PBE-D3-BJ for the inclusion of the van der Waals (vdWs) interactions. [31,32] The Scalar relativistic correction was used for the inclusion of relativistic effects [33]. In ADF-BAND module, the scalar relativistic effects are not purely first-order correction rather it is the quasi-relativistic approach. Considering the electronic configuration of Sb and O that are [Kr] $4d^{10}$ $5s^2$ $5p^3$ and [He] $2s^2$ $2p^4$, the frozen core was taken as "Large" that would freeze the core orbitals and to accelerate the calculation. The energy convergence criteria was chosen as $10^{-6}$ eV whereas gradient was $10^{-3}$Å.

The formation energy per atom of the materials was computed by using the formula

$$Formation\ energy \Big/ atom = \frac{products - reactants}{n} \quad .(1)$$

Provided that the number of atoms in reactant and product are same, where n is total number of atoms present. For instance, the formation energy per atom for unit cell could be written as

$$E_f = \frac{E(Sb_8O_{12}) - 4E(Sb_2) - 6E(0_2)}{n} \quad .(2)$$

Where n indicates the total number of atoms present in the system. Furthermore, the oxygen part in the formula was calculated by considering two cases, (i) the non-magnetic with spin zero, (ii) the paramagnetic behavior for which the spin value of 1 was included. The value of formation energy of $O_2$ was found smaller with spin 1 owing to the natural paramagnetic behavior. Hence, in order to find the formation energy of $Sb_2O_3$, the spin was included and the calculated values are given in Table 2.

Furthermore, the bonding of the materials were discussed by the electronegativity difference, Pauli formula and the covalent, ionic and vdWs radii [34]. In order to investigate the inter-cage interactions, the pEDA-NOCV calculations were performed at single point geometries. The GGA-PBE-D3-BJ level of theory were utilized and the remaining parameters were similar as for other calculations. The pEDA-NOCV were performed by considering only the 2 molecular units (cages) each as an independent fragment and the remaining atoms were deleted. The pEDA-NOCV calculations gives the several energy terms that aids in understanding the structure of the materials. The EDA decomposes the interaction energies of a molecule AB into two fragment A and B [35,36]. The interaction energy is the difference in energy between the molecule and the developed fragments (i.e. $E_A$, $E_B$), thus the interaction energy is written as the

$$\Delta E_{int} = E_{AB} - (E_A + E_B) = \Delta E_{pauli} + \Delta E_{elstat} + \Delta E_{orb}$$

Where the term $\Delta E_{Pauli}$ describes the exchange repulsion in between the fragments, which appears in consequence of the Pauli's principle while $\Delta E_{elastat}$ presents the quasiclassical electrostatic interaction energy in between the charge densities of the fragments. Moreover, the term $\Delta E_{Orb}$ explains the gain in energy due to the mixing of orbitals from the fragment. In addition to this, the $\Delta E_{steric}$ term is added that would present the steric interaction energy present in between them [37].

In order to model the interactions in $Sb_2O_3$, only two cages are considered for each periodicity such as the bulk, slab, chains and clusters in such a way that each cage is considered as a fragment/monomer as shown in Fig. 1 to shed light on the inter-cage interactions.

## 3. Results and discussion

### 3.1. Structural properties

The structural parameters are described on the basis of bond length, bond angles, bonding and the formation energy. The optimized structure for the bulk $Sb_2O_3$ is shown in Fig. 2. Unlike the usual bulk structures

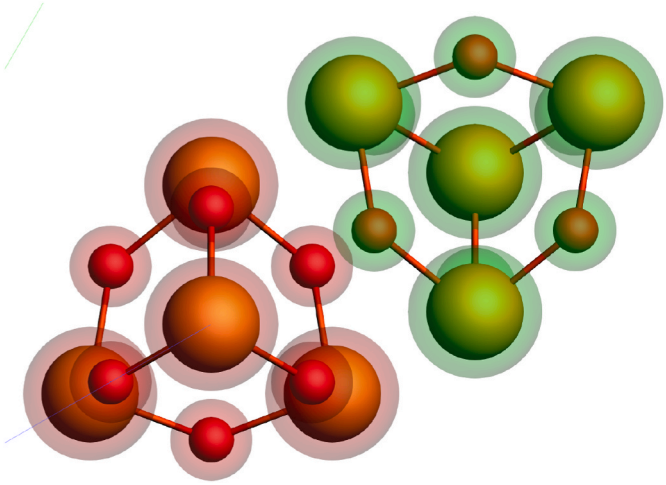

**Fig. 1.** The formation of fragments in $Sb_2O_3$ to perform the pEDA analysis.

with close packing, the relaxed structure exhibited some modification. In this structure, there exists the close cage structures and these cages spread out in regular manner in the three directions and all these cages are linked with the neighbors via vdWs interactions. This is obvious from the bond length analysis where inter-cage bond lengths (i.e. the bond length in between the cages) are different from the intra-cage bond length (bond length within a cage) as shown in Table 1. The intra-cage bond length is as follows, i.e. the bond length Sb–O is 2.047 Å and O–O is 3.08 Å where no metal-metal bond is observed while the inter cage bond lengths Sb–Sb and O–O are 3.07 Å and 4.04 Å respectively, hence the inter-cage distance is in the range of 3.07–4.04 Å. However, upon repeating the calculations with different functionals, no notable changes in bond lengths and bond angles were observed. The observed distinctions in values of bond lengths for inter-cages and intra-cages cages revealed anisotropy in the structures. Yet, in contrast to the customary vdWs material where there is anisotropy in the in-plane and out-of-plane bonding [38,39]; in the current material the anisotropy is observed throughout the material. Hence for the case of the bulk $Sb_2O_3$, there is the anisotropy in bonding in three dimension (3D) in line with the relevant literature [2].

Similarly, the 2D slab is optimized in two different ways. It is done by slicing the bulk along (111) plane and (001) plane [2]. Moreover, the chains and clusters are optimized accordingly, where (111) chains were optimized from the slab (111) and the cluster (111) were initiated from the chains (111) as shown in Fig. 3. The slicing along the specific plane was performed (i) to obtain the cages in the slab and lower dimensions and (ii) to attain most stable and hence most suitable configuration for future study. During the sequential downscaling, the obtained optimized bond lengths and bond angles are given in Table 1, as we can see that a decrease in bond length and bond angle is observed upon downscaling that is consistent with the relevant literature [33]. The observations revealed that no such impact on bond length and bond angles observed as by changing the functional. The anisotropy in bonding can be observed for all cases which indicates the presence of anisotropy regardless of the dimensions. Moreover, by slicing along the specific plane/direction, the cages can be structurally tuned as shown in the Fig. 1. Similarly, the structural parameters are computed for chains and clusters and given in Table 1 and anisotropy in bonding is observed similar to the previous cases.

#### 3.1.1. Formation energy analysis

The description of stability of materials at ambient conditions is important, while modelling the materials. Hence, the dynamical stability of the materials will be described in the following to know the dynamical stability based on phonon calculations.

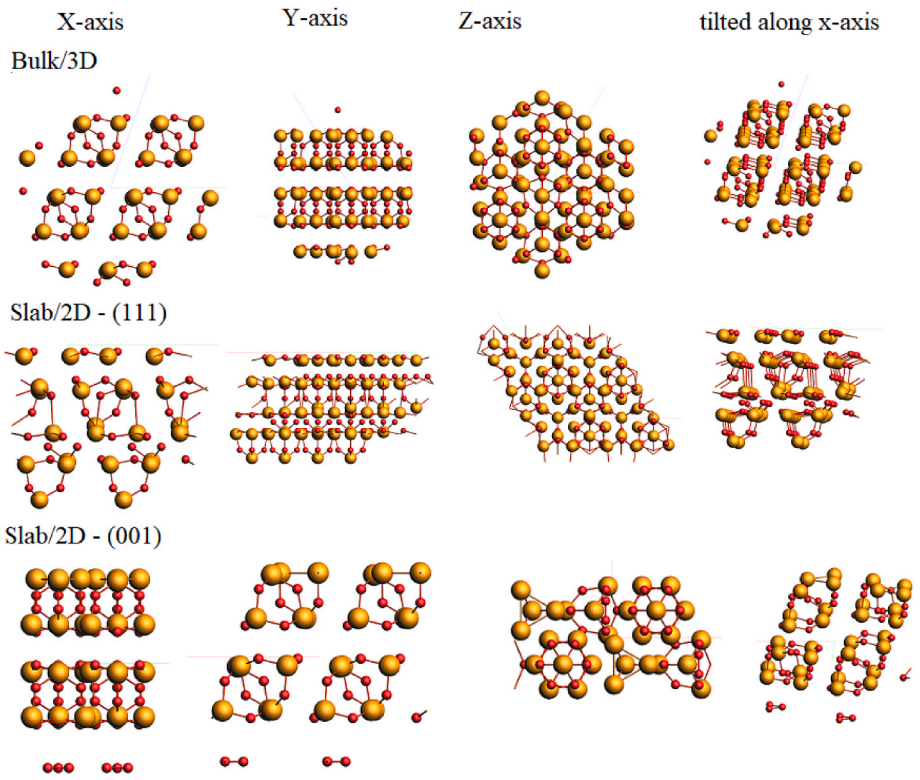


**Fig. 2.** The optimized structure of $Sb_2O_3$ in bulk/3D, slab/2D – (111) and slab (001) for the purpose of downscaling.

**Table 1**
The values of bond lengths and bond angles of bulk/3D, slab/2D, chains/1D and clusters/0D calculated at different levels of theory.

| Periodicity | Structure | Structural Properties | | | | |
|---|---|---|---|---|---|---|
| | | Sb–O (Å) | Sb–Sb (Å) | O–O (Å) | Sb–O–Sb (Degree) | O– Sb–O (Degree) |
| Bulk | GGA-PBE | 2.04–2.05 | 4.04 | 3.07–3.09 | 129.4 | 97.7 |
| | GGA-PBE-D3 | 2.049 | 4.04 | 3.07 | 129.9 | 97.7 |
| | GGA-PBE-D3-BJ | 2.049 | 4.04 | 3.08 | 128.8 | 98.8 |
| Slab (111) | GGA-PBE-D3 | 2.28, 2.06, 1.94 | 4.28 | 4.90 | 134, 128 | 93.7 |
| | GGA-PBE-D3-BJ | 2.20, 2.04, 2.03, 2.00 | 3.96 | 4.15 | 134 | 89.9 |
| Slab (001) | GGA-PBE-D3 | 2.03, 2.04, 2.05 | 4.01–4.02 | 4.28 | 129, 130 | 97.1, 98.3 |
| Chains from slab (111) | GGA-PBE-D3 | 2.04, 2.07, 2.08, 2.11, 2.20, 2.24 | | | | |
| Chains from slab (001) | GGA-PBE-D3 | 1.9, 2.02, 2.05, 2.20 | 3.8 | 2.63 | 129 | 96.3, 99.6 |
| Clusters from slab (111) | GGA-PBE-D3 | 1.94, 1.99, 2.00, 2.02, 2.03, 2.05, 2.11 | 3.26 | 2.62 | 98, 104 | 102 |
| Clusters from slab (001) | GGA-PBE-D3 | 2.05, 2.11 | 3.61 | 2.88 | 131 | 84.7, 90 |

The formation energy as computed using equation (1) for the various cases i.e. bulk, slab (111) and slab (001) as given in Table 2 per calculations using different levels of theory. For instance, for the unit-cell of bulk $Sb_2O_3$ having 20 atoms is given in equation (2).

Considering the possible paramagnetic response of oxygen in $Sb_2O_3$, the spin was taken into account while calculating the formation energy. The findings indicated paramagnetic behavior of $O_2$ molecule but no such effects were observed in case of $Sb_2O_3$ when calculations of formation energy was carried out at different levels of theory. Hence, $Sb_2O_3$ appeared non-magnetic as per agreement with the reported literature [24].

Considering the formation energy of $Sb_2O_3$, as this is clear that for each case, the energy is minimum as computed by the GGA-PBE-D3-BJ, which is considered as best inclusion and representation of vdWs interactions, and evident for the presence of the vdWs forces and the anisotropy in the structures. Moreover, by comparing different cases, the energy is minimum for the bulk $Sb_2O_3$ and shows that the most stable configuration is bulk/3D $Sb_2O_3$. Overall, the energy is more for the case of the slab as compared to the bulk but the energy is minimum for the slab (111) and hence shows most stable configuration and the slicing over (111) is most stable configuration out of the situations discussed here. Moreover, the clusters obtained direct from the bulk is least stable and the structure is distorted (not given here) so ignored for further studies.

The overall energy trend can be written as bulk < slab < chains < clusters, although the entire situations upon downscaling are possible but there is high possibility of transformation bulk to slab (111) and lower possibility of formation of clusters therefore we can conclude that there is lower chance of agglomeration and slabs/surfaces could be attained experimentally [33].

### 3.1.2. *Dynamical stability - phonons*

Besides the formation energy analysis, the phonon calculations were performed for bulk and surfaces as the phonons provide the insights regarding the dynamical stability of the materials through the lattice vibrations. In general, during the theoretical calculations, the atoms are considered as stationary/stick at a lattice point, but this is not true in actual cases. The atoms vibrate about their mean position to generate lattice vibrations [40].

The phonon band structures are calculated for bulk and surfaces i.e.

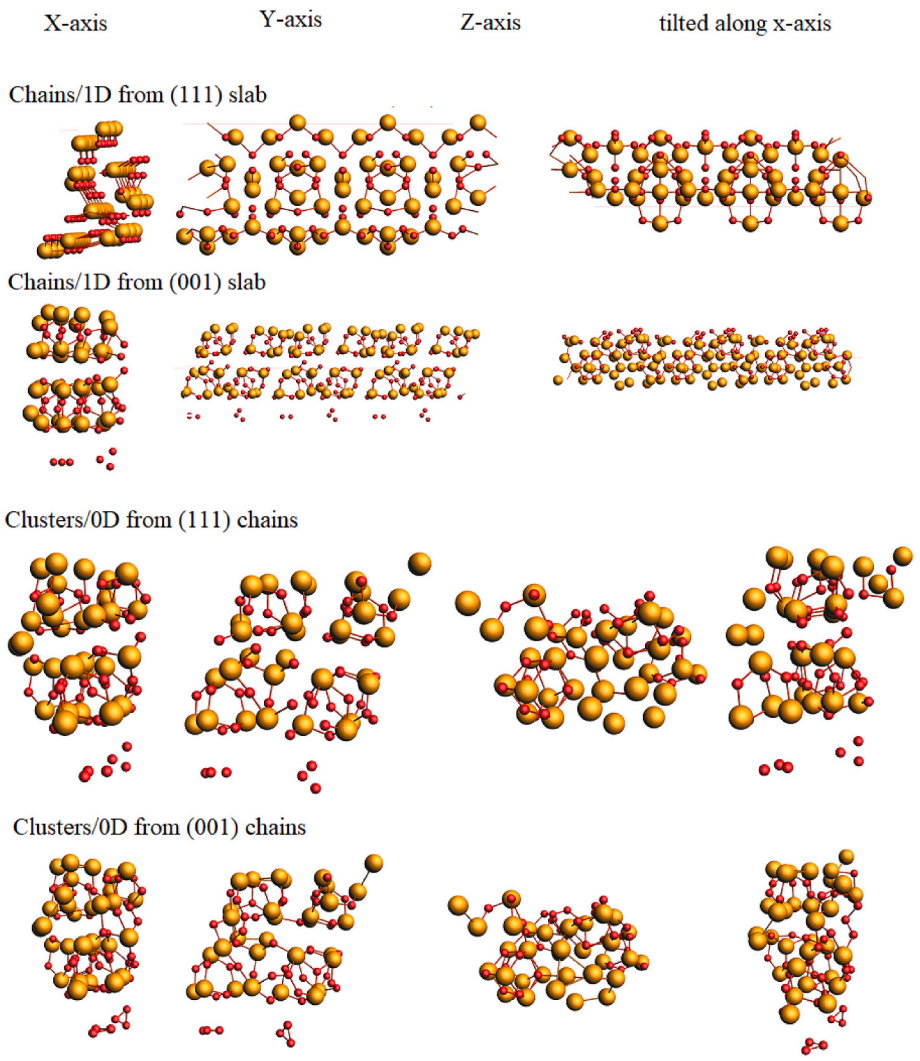


**Fig. 3.** The optimized structure of $Sb_2O_3$ in chains/1D chains (111) and chains (001), clusters/0D – (111) and clusters (001) for the purpose of downscaling.

**Table 2**
Formation energy (eV/atoms) determined for $Sb_2O_3$ at different levels of theory.

| Functional | Bulk | Slab (111) | Slab (001) | Chains from (111) slab | Chains from (001) slab | Clusters from (111) chains | Clusters from (001) chains | Clusters from Bulk |
|---|---|---|---|---|---|---|---|---|
| GGA-PBE | −1.19 | −1.04 | | −0.88 | −0.86 | −0.89 | | |
| GGA-PBE-D3 | −1.32 | −1.15 | −1.02 | −0.88 | −0.77 | −0.89 | −0.67 | |
| GGA-PBE-D3-BJ | −1.41 | −1.17 | −1.11 | −0.919 | −0.84 | −0.91 | | −0.152 |

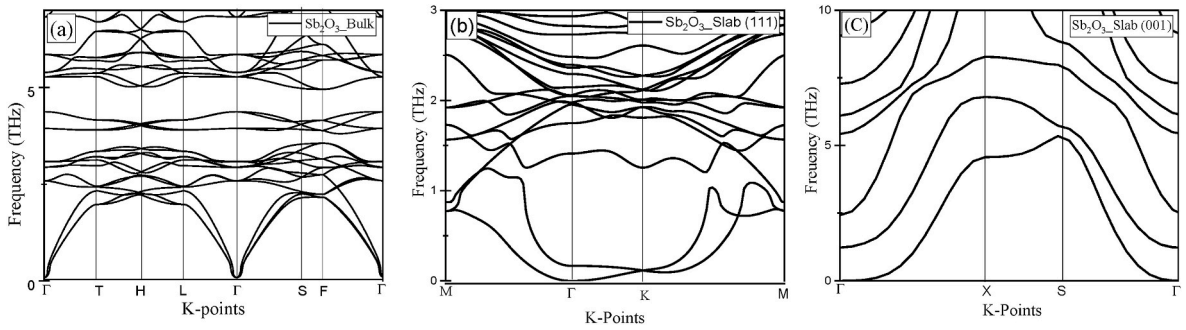


**Fig. 4.** The phonon band structure and their relevant partial density of states for (a) bulk, (b) slab (111) and (c) slab (001).

slab (111) and slab (001) as shown in Fig. 4 (a-c). Since the phonon branches are based on the number of atoms in the materials via relation i.e. number of phonon branches = 3 N, where N is the number of atoms in the structure. The material in bulk periodicity is comprised of 20 atoms, while in slab periodicity, the material's cell is comprised of 40 and 80 atoms for slab (111) and slab (001) respectively. Furthermore, the low frequency branches i.e. acoustic branches arise because of the heavier Sb atoms while the high frequency branches i.e. optical branches appeared due to the lighter O atoms in the material. Moreover, the frequency gap in phonon band structure is attributed to the mass difference between different atoms present in such a way that greater the mass difference, greater is the frequency gap [41,42]. Hence, the gap between the acoustic and optical branches are due to greater mass difference between the Sb and O atoms [43]. This is why, almost similar frequency gap is observed in the bulk, slab (111) and slab (001) structures of the material. Besides these, the highest phonon frequency of ~22 THz in bulk reveals the presence of strong bonding between the atoms of Sb and O [39]. Since only positive phonon branches are found and no negative branches appeared in case of the bulk and surfaces, these structures are stable which points to dynamical stability of materials. The finding is consistent with the literature as these materials have been experimentally synthesized [8].

### 3.1.3. Intercage interactions

The uniqueness of the IMCs lies on its structure, it will be interesting to understand the intra-cage and inter-cage interactions. Hence, in this sections, in addition to estimations based on theoretical knowledge, the findings on inter-cage and intra-cage interactions are given.

*3.1.3.1. Electron localization function (ELF) analysis.* The electron localization function (ELF) analysis is carried out to describe the localization of the electrons to help in understanding the primary bonding in the material. Hence the ELF analysis of the $Sb_2O_3$ materials at different periodicities was performed. The representative diagram showing the ELF density plots are given in Fig. 5. It appears that the primary bonding (i.e. strong covalent bonding) is present within the cages with absence of density between two cages pointing the absence of the primary bonding.

*3.1.3.2. pEDA-NOCV analysis.* Besides the explanation based on the bond lengths and relevant parameters, the explanation of the interaction between the molecular cages is helpful to explore the material's properties. The interaction between the two molecular cages in different cases i.e. bulk, slab, chains and clusters is presented on the basis of periodic energy decomposition analysis (pEDA). The aforementioned analysis is used to investigate the interaction within the system that especially includes the non-bonding interactions. To perform the pEDA analysis, the material is divided into the multiple fragments (in which the interactions are being studied) and then interactions are studied in between these fragment. In the framework of the pEDA analysis, we intended to address the inter-cage interactions for which each molecular unit (cage) in the IMCs must be considered as an independent fragment. Hence, in this perspective, only two cages are considered for each case i. e. bulk, slab, chains and clusters and then each cage is considered as fragment and the inter-cage and intra-cage interactions are investigated.

i. Bulk

The calculated orbital energy is the sum of the kinetic energy (T), electrostatic (Elast) energy and exchange correlation energy (XC) of above described fragments whose values are −29.181 eV, 24.789 eV, 3.337 eV. The overall orbital energy is −1.055 eV, indicating the fact the overall orbital energy is attractive in nature. Similarly, the steric interaction energy term is composed of the kinetic energy (T), electrostatic (Elast) energy and exchange correlation energy (XC), where the values are the 34.948 eV, −28.744 eV and −6.069 eV respectively [36]. The value of the total steric interaction energy is 0.134 presenting that the steric interaction is attractive in nature. The overall energy of the system is interaction energy ($\Delta E_{int}$). The computed values of the $\Delta E_{int}$ is −1.402 eV which is sum of the electrostaic, Pauli, dispersion and orbital energy where the values of $\Delta E_{Elastat}$, $\Delta E_{Pauli}$, $\Delta E_{dis}$ and $\Delta E_{Orb}$ are −2.928 eV, 3.062 eV, −0.481 eV, and −1.055 eV respectively [30,35,37].

The purpose of giving all the energy terms is to provide an insight into nature of the interaction present between them. The computed values indicate that both attractive (indicated by negative sign) and repulsive (positive sign) energy terms are present which balance each other and keeps the cages at their equilibrium/optimized separation to restrict them for coming further closer. Hence, the computed values of interaction energy indicates the equilibrium caused by balance of the attractive and repulsive forces between the cages [30,37].

ii. Slab

Alike to the bulk $Sb_2O_3$, the pEDA analysis were performed for its 2D slab which contains the similar structural anisotropy as that of its bulk/3D counterpart. The value of orbital energy was −1.055 which is sum of −28.939 eV, 24.551 eV and 3.333 eV representing the kinetic, electrostatic and exchange correlation terms respectively. Similar to these, the steric interaction between the orbitals was computed as 0.141 eV, which points to combined kinetic, electrostatic and exchange correlation terms having values of 34.949 eV, −28.739 eV and −6.069 eV respectively. It appears that the kinetic energy term is repulsive while the electrostatic and correlation terms are attractive that gives rise to overall repulsive term for the steric interaction. Hence it is concluded that the steric interaction is repulsive in nature. The bonding energy terms i.e. $\Delta E_{int}$ which is constituted as the $\Delta E_{Elastat}$, $\Delta E_{Pauli}$, $\Delta E_{dis}$ and $\Delta E_{Orb}$ having the respective values −2.920 eV, 3.061 eV, −0.477 eV and −1.055 eV give rise to total interaction energy as −1.390 eV [36]. Hence, the electrostatic, dispersion and the orbital energies are attractive while the Pauli energy term is repulsive in nature that causes an overall attractive energy term. It is therefore found that, in between the two cages, in case of 2D/slab periodicity, although the attractive term dominates but both the attractive and repulsive terms are present which balance each other to

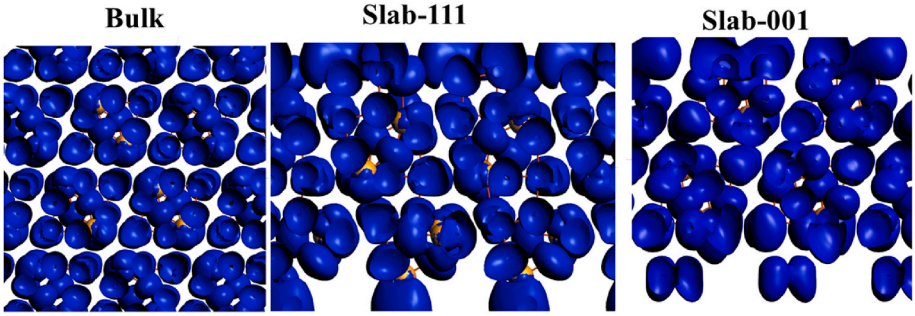


**Fig. 5.** The representative diagram of ELF analysis of the bulk, slab-111 and slab-001 facing the cages.

cause equilibrium [30,37].

iii. Chains

In case of chains the total steric interaction energy is 0.141 eV while total orbital interaction energy is −1.054 eV which indicate that steric interactions and orbital energies are repulsive and attractive respectively. Moreover, the computed interaction energy is −1.387 eV, whereas the value of Pauli energy, dispersion energy, electrostatic energy and orbital energy are 3.062 eV, −0.473 eV, −2.922 eV and −1.054 eV respectively. Similar to the previous case, the attractive terms dominant and the results are in agreement with the previous cases.

iv. Clusters

Similar to previous cases, the pEDA analysis were performed for the clusters/quantum dots with zero dimensionality. The steric interaction energy computed was equal to the 0.141 where the calculated values for the kinetic, electrostatic and exchange correlation energy were 34.948 eV, −28.740 eV and −6.067 eV respectively. Furthermore, the orbital energy values are −28.897 eV, 24.522 eV and 3.320 eV for the kinetic, electrostatic and exchange correlation part respectively owns a value of ~ −1.054 eV that is attractive in nature [36]. Moreover, talking about the main bonding energy terms, the interaction energy is −1.385 eV, that comprise of the values of the 3.062 eV for the Pauli energy term, −0.471 eV for energy dispersion term, −2.921 eV for the electrostatic energy term and −1.054 eV for orbital energy term. It is concluded that, similar to previous cases, the interaction energy terms are attractive in nature that helps to stay the molecular units as an independent units and there are non-covalent bonding type interaction presents that make them stay within a single structure.

By comparing the respective energy terms from 3D, 2D, 1D and 0D i. e. bulk, slab, chains and clusters, it is clear that there is minor difference in the energy terms that may be associated to the fact that only two cages were considered and interactions were investigated in between the two cages. Another reason may be due to the fact that there is a minute difference in inter-cage distance as moving from the bulk to slab, chains and cluster. Conclusively, the pEDA analysis is carried out to investigate the non-covalent inter-cage interactions which are found unchanged by structurally downscaling $Sb_2O_3$ from 3D to 0D.

### 3.2. Electronic properties

The electronic properties of the investigated materials are specified in terms of total and partial density of states as well as band structures. The electronic properties were calculated at GGA-PBE, GGA-PBE-D3, GGA-PBE-D3-BJ and TB-mBJ levels of theory but the DOS and band structures computed by GGA-PBE-D3-BJ are plotted here and a comparison with the other methods is provided.

i. Bulk $Sb_2O_3$

The partial DOS chart of bulk $Sb_2O_3$ is depicted in Fig. 6, where DOS is plotted as a function of energy in eV. The position of Fermi level is shifted to 0 eV and is represented by blue dotted line. The respective regions on the right and left sides of the Fermi level are conduction band (CB) and valence band (VB). The black line represents the total DOS from the material while red and blue colors exhibit the total contribution from the Sb and O respectively. The analysis of DOS indicates that the material is wide gap semiconductor with a band gap of 3.39 eV that is in consistent with the relevant literature [2].

The orbitals in the VB are occupied which emerged mostly from the bonding orbitals and hence have lower energy. On the other hand, the orbitals in the CB are unoccupied, originated from non-bonding orbitals and hence placed at higher energy. The CBM (conduction band minima) and VBM (valence band maxima) is formed by the hybridization of

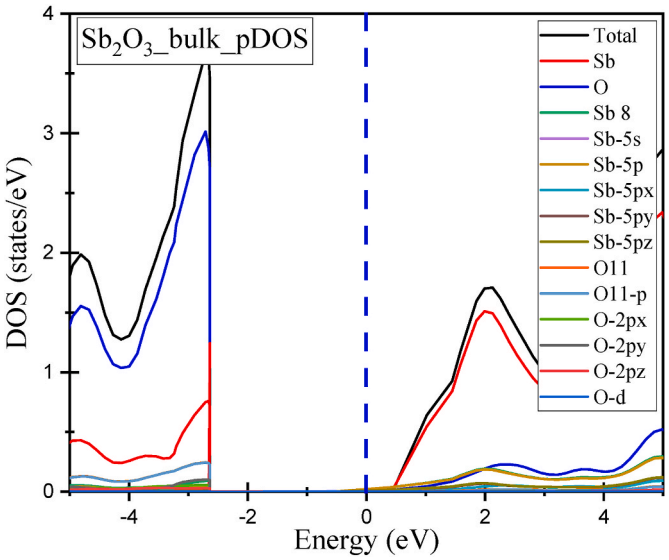


**Fig. 6.** The DOS calculated for the bulk $Sb_2O_3$; where the Fermi level is shifted to 0 eV and is represented by blue dotted line.

orbitals from the Sb and O atoms respectively. The major contributions in formation of respective CB and VB appeared from Sb and O [44]. The closer inspection of the DOS revealed a hybridization of Sb-5p and even Sb-5s orbitals with oxygen orbitals in the VB. The Sb-$5p_x$ is hybridized with O-$2p_y$ to produce the sigma (σ) bonding orbitals exhibiting presence of other orbital hybridization. Similarly, in the CB, the Sb-$5p_y$ hybridized with O-$2p_z$ leading to the formation of π bond. This is evident for the formation of π bonds in conduction and valence bond.

For the further details, the band structure is plotted and showed in Fig. 7; and the Brillouin zone formed is cubic with K-points following the path Γ, X, W, K, Γ, L, U, W, L, K and U. The VBM and CBM are found at Γ and X points respectively which points to indirect wide band gap semiconductor with the band gap 3.39 eV that is in agreement with literature [45]. Hence, inter band electronic transitions in the material triggered by photons must be phonon assisted.

ii.(111) Slab of $Sb_2O_3$

The chart showing total and partial DOS computed for slab (111) is given in Fig. 8 where the Fermi level is set at 0 eV and is represented

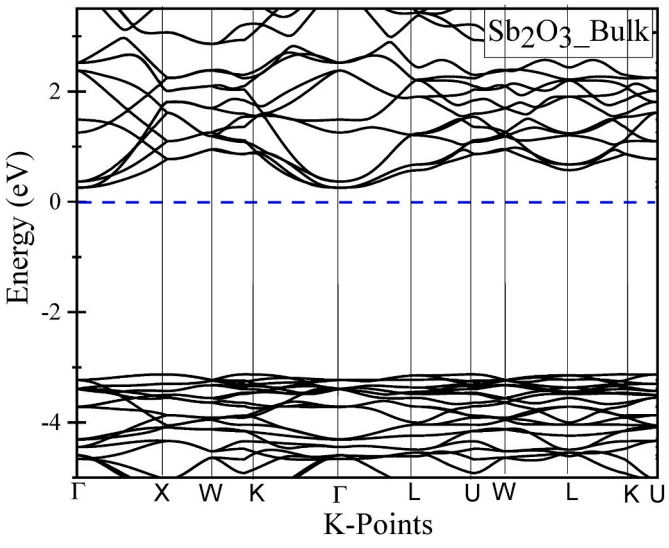


**Fig. 7.** The band diagram for the bulk $Sb_2O_3$, where the Fermi level is shifted at 0 eV and represented by blue dotted line.

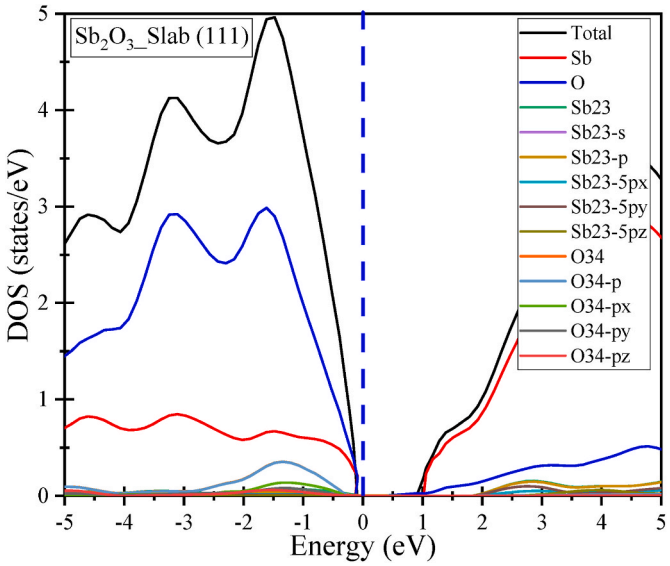


**Fig. 8.** The total and partial density of states (pDOS) computed for the slab in (111) plane, where the black colored states represent the total DOS while the red and blue colored states shows the total contribution from Sb and O respectively.

by the dotted line in blue color. The oxygen and Sb atoms form the VB and CB respectively, where the 5p from Sb shows the major contribution in CB while O-2p and its sub-orbitals from major part of VB. Since the Fermi level is somehow shifted towards the VB so, the material can be termed as semiconductor with a band gap of about 1.40 eV. Moreover, by looking more closely to the states, it was found that there is p-p hybridized states present in the VB and CB. In VB, the O-2$p_x$ states hybridize with Sb-5$p_z$ and Sb-5s orbital and besides hybridized orbitals there is the presence of π bond. There is smaller probability of formation of σ bond due to low density of p-orbitals on sides of the slab to produce head on overlapping. Similarly, in the CB, p-p hybridization is present which indicates existence of π anti-bonding molecular orbitals.

The band structure for the slab (111) is shown in Fig. 9, in which the Brillouin zone is cubic and follows the path Γ, M, K. The results reveal

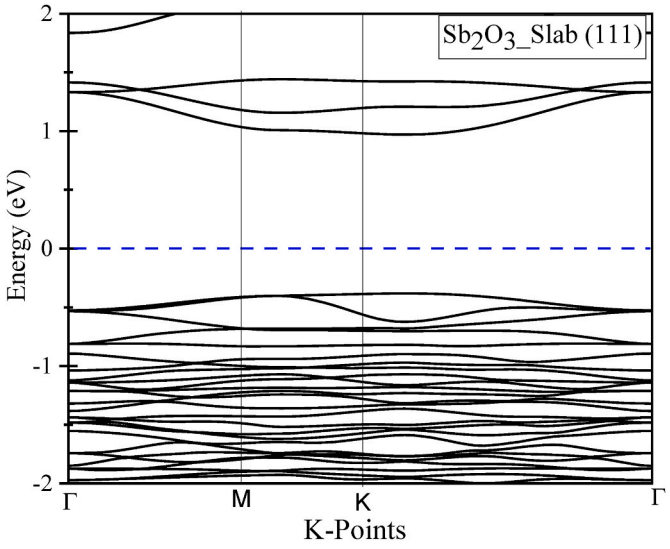


**Fig. 9.** The band diagram for the slab (111) of $Sb_2O_3$, where the Fermi level is shifted at 0 eV and represented by blue dotted line.

that the material is a pure semiconductor with a direct band gap of about 1.4 eV as the both VBM and CBM occurs at K-point. This indicate that the movement of electron from VB to CB requires a photon of having energy equal or greater than 1.40 eV.

The partial DOS for the slab trimmed in (001) plane is shown in Fig. 10, where the fermi level is shifted at 0 eV and represented by the blue dash-dotted line. Here, as we can see that the material shows the semiconducting behavior with a band gap of about 1.04 eV. Moreover, similar to the previous case, the Sb and O atoms hybridize and their hybridized states are present with major contribution of Sb and O in CB and VB respectively.

iii.$Sb_2O_3$ chains (111)

The total and partial DOS for the chains as obtained by the downscaling of the slab (111) and denoted by chains (111) is given in Fig. 11, where the total DOS are depicted by the black line whereas the red and blue line represents the total contribution of Sb and O atoms respectively. The results points to semiconducting nature of the material with a band gap of 1.37 eV. Moreover, there is the p-p hybridization states present both in CB and VB. In case of the VB, the major contribution arises from the oxygen atoms while in CB the major contribution arises hybridization appeared from the Sb atoms. Furthermore, close to Fermi level in the VB, hybridization 2$p_x$ -2$p_z$ and 2$p_x$ -5$p_x$ appeared which points to the presence of sigma bond in valence molecular orbitals. Nevertheless, there is the 5$p_z$-5$p_y$ and 5$p_y$-5$p_x$ hybridization and in-turn presence of the π bonds in the CB i. e. anti-molecular π orbital is formed. Hence, the electronic structure of the chains (111) consists of the σ bonding molecular orbital and anti-bonding π molecular orbital.

iv. $Sb_2O_3$ Clusters (111)

Similar to previous cases, the total and partial DOS of clusters as obtained by the downscaling of the chains (111) and denoted by clusters (111). The results obtained showed that the material is semiconductor with a band gap of 1.8 eV. Now, since there is p-p hybridization in VB and CB with maximum contribution from Sb in CB and by O in VB. Also, in VB, there is 5$p_x$-5$p_z$ and 5$p_z$-5$p_y$ hybridization and hence presence of the π molecular orbitals. Furthermore, in CB there is a prominent 5$p_y$-5$p_z$ hybridization, so it is evident of π anti-molecular orbital. Besides these, the states obtained in case of chains and clusters are sharp, this is due to the

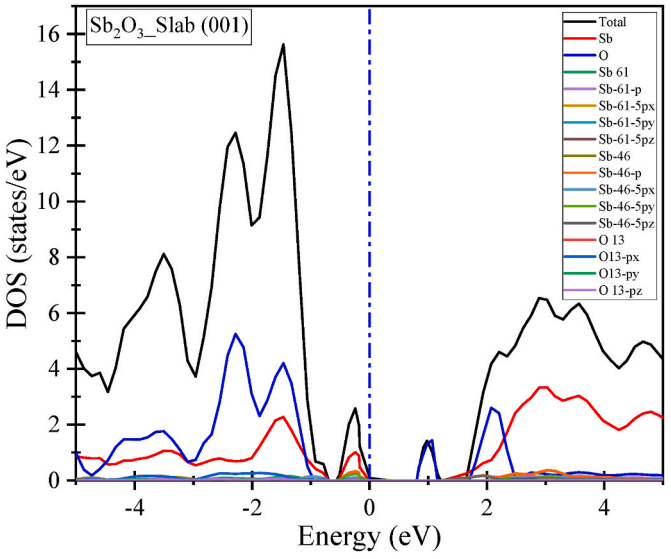


**Fig. 10.** The total and partial density of states (pDOS) computed for the slab in (001) plane of $Sb_2O_3$, where the black colored states represent the total DOS while the red and blue colored states shows the total contribution from Sb and O respectively.

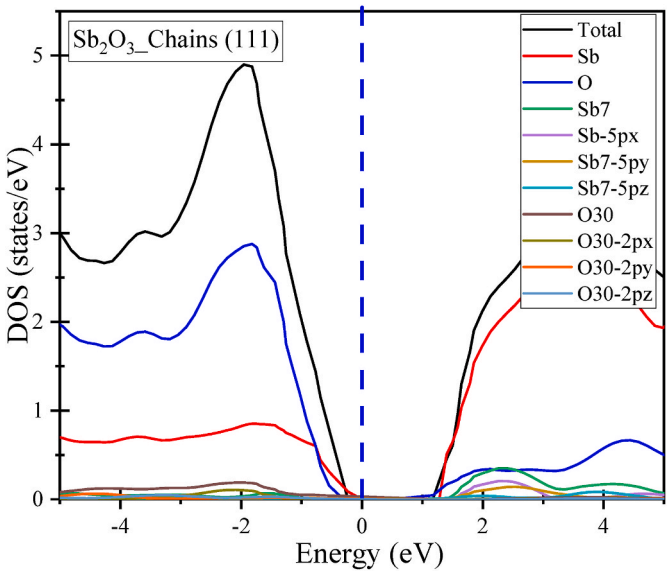


**Fig. 11.** The total and partial density of states (pDOS) computed for the chains from slab (111) $Sb_2O_3$.

quantum confinement effect. This arises because the atoms are comparatively less surrounded and hence no formation of bands rather they exist as the atomic states (in case of clusters).

The electronic properties for different cases revealed that bulk, slab (111) and slab (001) presents the semiconducting behavior with a band gap of ~3.38 eV, 1.40 eV and 1.04 eV respectively. There are p-p hybridized states from Sb and O present within the VB and CB with the major contribution of Sb and O atoms within the CB and VB respectively.

Besides overall discussion, the band gap for different situations are given in Table 3 which indicates that the band-gap obtained by the GGA-PBE-D3-BJ is very close to the experimental value for slabs (~3.5–4 eV) and the band gap as computed by the TB-mBJ functional is 4.63 eV that is close to the experimental values reported in different studies [41,46]. Furthermore, the comparison of the values indicated that the band gap decreases as the structures are downscaled [25].

v. Relation between the electronic properties of Bulk and 2D materials

The electronic properties of the $Sb_2O_3$ in the bulk and lower dimensions are described in details in the previous sections. Here, we are going to give comparative picture of electronic properties of the material in bulk and 2D. The bulk $Sb_2O_3$ is an indirect band gap semiconductor as the VBM occurs at K-points and the CBM occurs at the $\gamma$-point whereas in case of 2D $Sb_2O_3$, in the form of slabs (111) and (001), it appeared as direct band gap where the VBM and CBM lies at K-points in the band diagram. Thus, there is a transition from indirect to direct band gap as we move from bulk to 2D periodicity and trend is similar to the TMDs for instance $MoS_2$ [47,48],$WS_2$ [49,50], $MoSe_2$ [51], $WSe_2$ [52].

**Table 3**
The band gap values (eV) as calculated by different functional.

| Functional | Bulk | Slab (111) | Slab (001) | Chains (111) | Chains (001) | Clusters (111) |
|---|---|---|---|---|---|---|
| GGA-PBE | 3.34 | 1.40 | 1.04 | 1.37 | 0.41 | 1.30 |
| GGA-PBE-D3 | 3.34 | 1.03 | 1.09 | 1.37 | 1.09 | 0.73 |
| GGA-PBE-D3-BJ | 3.39 | 1.40 | 1.05 | 1.37 | 0.412 | 1.8 |
| TB-mBJ | 4.63 | 1.96 | 4.23 | 2.52 | 1.60 | 2.25 |

Furthermore, the band gap of the material appeared to decreases when $Sb_2O_3$ is downscaled from bulk to the slabs i.e. the band gap decreases by a value of 1.99 and 2.34 for slab (111) and slab (001) respectively.

## 4. Summary

The 3D anisotropy being a specific attribute of inorganic molecular crystals (IMCs) has been observed in the structure of $Sb_2O_3$. The structural and electronic properties of 3D (bulk), 2D (slab (111), slab (001)), 1D (chains (111) and chains (001)) and 0D (clusters (111) and clusters (001)) are discussed in details. The uniqueness of the IMCs lie in their specific structures i.e. covalently bonded cage structure and vdWs interaction in between the cages and to deal with that the dispersion functional as given by Grimm's (i.e. D3) and then corrected by Backe-Johnsons (D3-BJ) (both Grimm's and Corrected) are considered to investigate the properties. The effects of structural downscaling on the properties of the materials are discussed in detail. In this case, the slabs are trimmed along (111) and (001) planes and subsequent downscaling is carried out. The structural properties revealed that the bond-lengths decreases as the dimension decreases. The pEDA analysis revealed the presence of inter-cage interactions that keeps these cages linked with each other. These interactions, as computed by the interaction energy, are based on both attractive and repulsive nature that balances each other's impact and it's the attractive energy terms that dominates in each case (i.e. 3D, 2D, 1D and 0D), hence the interactions between the molecular cages would be more attractive than repulsive. Furthermore, the formation energy analysis provide information regarding the stability of materials and gave the prospects regarding the possibility of conversion to related lower dimension, while the phonon calculations put light on the dynamical stability and confirmed the stability of materials. The electronic properties for different cases revealed that bulk, slab (111) and slab (001) presents the semiconducting behavior with a band gap of ~3.38 eV, 1.40 eV and 1.04 eV respectively. There are p-p hybridized states from Sb and O present within the VB and CB with the major contribution of Sb and O atoms within the CB and VB respectively.

## Ethical approval

Not applicable.

## Funding

The authors sincerely appreciate funding from Researchers Supporting Project number (RSP2023R399), King Saud University, Riyadh, Saudi Arabia.

## Availability of data and materials

Not applicable.

## CRediT authorship contribution statement

**Alia Jabeen:** Writing – original draft, Methodology, Investigation, Formal analysis. **Abdul Majid:** Writing – review & editing, Supervision, Methodology, Conceptualization. **Mohammad Alkhedher:** Writing – review & editing, Visualization, Validation, Methodology. **Sajjad Haider:** Writing – review & editing, Visualization, Validation. **Muhammad Saeed Akhtar:** Writing – review & editing, Visualization, Validation.

## Declaration of competing interest

The authors declare that they have no known competing financial interests or personal relationships that could have appeared to influence the work reported in this paper.

## Data availability

Data will be made available on request.

## References


[1] M. Xiao, et al., Sub-5 nm single crystalline organic p–n heterojunctions, Nat. Commun. 12 (1) (2021) 2774.
[2] K. Liu, L. Liu, T. Zhai, Emerging two-dimensional inorganic molecular crystals: the concept and beyond, J. Phys. Chem. Lett. 13 (9) (2022) 2173–2179.
[3] B. Guo, et al., 2D layered materials: synthesis, nonlinear optical properties, and device applications, Laser Photon. Rev. 13 (12) (2019), 1800327.
[4] F. Liu, et al., Synthesis of graphene materials by electrochemical exfoliation: recent progress and future potential, Carbon Energy 1 (2) (2019) 173–199.
[5] M.S.A. Bhuyan, et al., Synthesis of graphene, Int. Nano Lett. 6 (2016) 65–83.
[6] F. Wang, et al., Two-dimensional non-layered materials: synthesis, properties and applications, Adv. Funct. Mater. 27 (19) (2017), 1603254.
[7] J. Bai, A.V. Virovets, M. Scheer, Synthesis of inorganic fullerene-like molecules, Science 300 (5620) (2003) 781–783.
[8] W. Han, et al., Two-dimensional inorganic molecular crystals, Nat. Commun. 10 (1) (2019) 1–10.
[9] M. Hu, et al., Reversible conversion-alloying of Sb2O3 as a high-capacity, high-rate, and durable anode for sodium ion batteries, ACS Appl. Mater. Interfaces 6 (21) (2014) 19449–19455.
[10] Y. Tan, et al., Synthesis of a symmetric bundle-shaped Sb2O3 and its application for anode materials in lithium ion batteries, Mater. Lett. 212 (2018) 103–106.
[11] K. Liu, et al., Wafer-scale van der Waals Dielectrics of Inorganic Molecular Crystals, 2021.
[12] M. Raupach, R. Tonner, A periodic energy decomposition analysis method for the investigation of chemical bonding in extended systems, J. Chem. Phys. 142 (19) (2015), 194105.
[13] M.v. Hopffgarten, G. Frenking, Energy decomposition analysis, Wiley Interdiscip. Rev. Comput. Mol. Sci. 2 (1) (2012) 43–62.
[14] K. Kitaura, K. Morokuma, A new energy decomposition scheme for molecular interactions within the Hartree-Fock approximation, Int. J. Quant. Chem. 10 (2) (1976) 325–340.
[15] T. Ziegler, A. Rauk, A theoretical study of the ethylene-metal bond in complexes between copper (1+), silver (1+), gold (1+), platinum (0) or platinum (2+) and ethylene, based on the Hartree-Fock-Slater transition-state method, Inorg. Chem. 18 (6) (1979) 1558–1565.
[16] A. Nilsson, L.G. Pettersson, J. Norskov, Chemical Bonding at Surfaces and Interfaces, Elsevier, 2011.
[17] B.D. Dunnington, J. Schmidt, Generalization of natural bond orbital analysis to periodic systems: applications to solids and surfaces via plane-wave density functional theory, J. Chem. Theor. Comput. 8 (6) (2012) 1902–1911.
[18] T.R. Galeev, et al., Solid state adaptive natural density partitioning: a tool for deciphering multi-center bonding in periodic systems, Phys. Chem. Chem. Phys. 15 (14) (2013) 5022–5029.
[19] X. Fang, et al., Inorganic semiconductor nanostructures and their field-emission applications, J. Mater. Chem. 18 (5) (2008) 509–522.
[20] X.-S. Fang, et al., Regular MgO nanoflowers and their enhanced dielectric responses, Appl. Phys. Lett. 88 (1) (2006), 013101.
[21] X.S. Fang, et al., Twinning-mediated growth of Al2O3 nanobelts and their enhanced dielectric responses, Adv. Mater. 17 (13) (2005) 1661–1665.
[22] Z.L. Wang, Zinc oxide nanostructures: growth, properties and applications, J. Phys. Condens. Matter 16 (25) (2004) R829.
[23] A. Majid, M. Bibi, Cadmium based II-VI semiconducting nanomaterials, Gewerbestrasse 11 (2018) 6330.
[24] W. Han, et al., Two-dimensional inorganic molecular crystals, Nat. Commun. 10 (1) (2019) 4728.
[25] J. Li, et al., In-plane crystal field constrained electronic structure of stanene, Appl. Phys. Lett. 116 (10) (2020), 101601.
[26] P. Zhang, et al., Topological and electronic transitions in a Sb (111) nanofilm: the interplay between quantum confinement and surface effect, Phys. Rev. B 85 (20) (2012), 201410.
[27] Y. Wu, et al., Inorganic semiconductor nanowires: rational growth, assembly, and novel properties, Chem.–Eur. J. 8 (6) (2002) 1260–1268.
[28] V.P. Sharma, et al., Advance applications of nanomaterials: a review, Mater. Today: Proc. 5 (2) (2018) 6376–6380.
[29] A. Bratovcic, Different applications of nanomaterials and their impact on the environment, SSRG International Journal of Material Science and Engineering 5 (1) (2019) 1–7.
[30] A. Majid, et al., On the prospects of layeredness in tantalum pentoxide, Mater. Sci. Eng., B 272 (2021), 115349.
[31] W. Reckien, et al., Implementation of empirical dispersion corrections to density functional theory for periodic systems, J. Comput. Chem. 33 (25) (2012) 2023–2031.
[32] P. Hyldgaard, Y. Jiao, V. Shukla, Screening nature of the van der Waals density functional method: a review and analysis of the many-body physics foundation, J. Phys. Condens. Matter 32 (39) (2020), 393001.
[33] A. Jabeen, et al., On downscaling of the tantalum oxides from three to zero dimensions, Mater. Sci. Semicond. Process. 151 (2022), 107014.
[34] S.S. Batsanov, Van der Waals radii of elements, Inorg. Mater. 37 (9) (2001) 871–885.
[35] P.T. Mathew, F. Fang, Periodic energy decomposition analysis for electronic transport studies as a tool for atomic scale device manufacturing, Int. J. Extrem. Manuf. 2 (1) (2020), 015401.
[36] L. Zhao, et al., Energy decomposition analysis, Wiley Interdiscip. Rev. Comput. Mol. Sci. 8 (3) (2018) e1345.
[37] A.D. Wonanke, M.A. Addicoat, Effect of unwanted guest molecules on the stacking configuration of covalent organic frameworks: a periodic energy decomposition analysis, Phys. Chem. Chem. Phys. 24 (25) (2022) 15494–15501.
[38] X. Ling, et al., Raman enhancement effect on two-dimensional layered materials: graphene, h-BN and MoS2, Nano Lett. 14 (6) (2014) 3033–3040.
[39] R. Ganatra, Q. Zhang, Few-layer MoS2: a promising layered semiconductor, ACS Nano 8 (5) (2014) 4074–4099.
[40] M. Klein, G. Horton, The rise of self-consistent phonon theory, J. Low Temp. Phys. 9 (1972) 151–166.
[41] F.L. Thiemann, et al., Machine learning potential for hexagonal boron nitride applied to thermally and mechanically induced rippling, J. Phys. Chem. C 124 (40) (2020) 22278–22290.
[42] Yu, X., et al., Anomalous Lattice Thermal Conductivity in Layered Materials MNCl (M= Zr, Hf) Driven by the Lanthanide Contraction.
[43] M. Azmat, et al., A first-principles study on two-dimensional tetragonal samarium nitride as a novel photocatalyst for hydrogen production, Int. J. Hydrogen Energy (2023), https://doi.org/10.1016/j.ijhydene.2023.04.248.
[44] M.H. Lakhdar, Y.B. Smida, M. Amlouk, Synthesis, optical characterization and DFT calculations of electronic structure of Sb2O3 films obtained by thermal oxidation of Sb2S3, J. Alloys Compd. 681 (2016) 197–204.
[45] H. Shiel, et al., Band alignment of Sb2O3 and Sb2Se3, J. Appl. Phys. 129 (23) (2021), 235301.
[46] K. Liu, et al., A wafer-scale van der Waals dielectric made from an inorganic molecular crystal film, Nature Electronics 4 (12) (2021) 906–913.
[47] S. Ahmad, S. Mukherjee, A Comparative Study of Electronic Properties of Bulk MoS2 and its Monolayer Using DFT Technique: Application of Mechanical Strain on MoS2 Monolayer, 2014.
[48] Q. Yue, et al., Mechanical and electronic properties of monolayer MoS2 under elastic strain, Phys. Lett. 376 (12–13) (2012) 1166–1170.
[49] D. Muoi, et al., Electronic properties of WS2 and WSe2 monolayers with biaxial strain: a first-principles study, Chem. Phys. 519 (2019) 69–73.
[50] H. Sahin, et al., Anomalous Raman spectra and thickness-dependent electronic properties of WSe 2, Phys. Rev. B 87 (16) (2013), 165409.
[51] C. Ghosh, et al., Equibiaxial strain: tunable electronic structure and optical properties of bulk and monolayer MoSe2, J. Phys. Appl. Phys. 46 (39) (2013), 395304.
[52] J. Gusakova, et al., Electronic properties of bulk and monolayer TMDs: theoretical study within DFT framework (GVJ-2e method), Phys. Status Solidi 214 (12) (2017), 1700218.